

Elastic properties of majoritic garnet inclusions in diamonds and the seismic signature of pyroxenites in the Earth's upper mantle

IULIA KOEMETS¹, NICCOLÒ SATTA^{1,†}, HAUKE MARQUARDT^{1,2}, EKATERINA S. KISEEVA^{2,3,*},
ALEXANDER KURNOSOV¹, THOMAS STACHEL⁴, JEFF W. HARRIS⁵, AND LEONID DUBROVINSKY¹

¹Bayerisches Geoinstitut, University of Bayreuth, 95440 Bayreuth, Germany

²University of Oxford, Department of Earth Sciences, South Parks Road, Oxford, OX1 3AN, U.K.

³University College Cork, School of Biological, Earth and Environmental Sciences, Distillery Fields, North Mall, Cork T23 N73K, Ireland

⁴Department of Earth and Atmospheric Sciences, University of Alberta, Edmonton, Alberta T6G 2E3, Canada

⁵School of Geographical and Earth Sciences, University of Glasgow, Glasgow G12 8QQ, U.K.

ABSTRACT

Majoritic garnet has been predicted to be a major component of peridotite and eclogite in Earth's deep upper mantle (>250 km) and transition zone. The investigation of mineral inclusions in diamond confirms this prediction, but there is reported evidence of other majorite-bearing lithologies, intermediate between peridotitic and eclogitic, present in the mantle transition zone. If these lithologies are derived from olivine-free pyroxenites, then at mantle transition zone pressures majorite may form monomineralic or almost monomineralic garnetite layers. Since majoritic garnet is presumably the seismically fastest major phase in the lowermost upper mantle, the existence of such majorite layers might produce a detectable seismic signature. However, a test of this hypothesis is hampered by the absence of sound wave velocity measurements of majoritic garnets with relevant chemical compositions, since previous measurements have been mostly limited to synthetic majorite samples with relatively simple compositions. In an attempt to evaluate the seismic signature of a pyroxenitic garnet layer, we measured the sound wave velocities of three natural majoritic garnet inclusions in diamond by Brillouin spectroscopy at ambient conditions. The chosen natural garnets derive from depths between 220 and 470 km and are plausible candidates to have formed at the interface between peridotite and carbonated eclogite. They contain elevated amounts (12–30%) of ferric iron, possibly produced during redox reactions that form diamond from carbonate. Based on our data, we model the velocity and seismic impedance contrasts between a possible pyroxenitic garnet layer and the surrounding peridotitic mantle. For a mineral assemblage that would be stable at a depth of 350 km, the median formation depth of our samples, we found velocities in pyroxenite at ambient conditions to be higher by 1.9(6)% for shear waves and 3.3(5)% for compressional waves compared to peridotite (numbers in parentheses refer to uncertainties in the last given digit), and by 1.3(13)% for shear waves and 2.4(10)% for compressional waves compared to eclogite. As a result of increased density in the pyroxenitic layer, expected seismic impedance contrasts across the interface between the monomineralic majorite layer and the adjacent rocks are about 5–6% at the majorite-eclogite-interface and 10–12% at the majorite-peridotite-boundary. Given a large enough thickness of the garnetite layer, velocity and impedance differences of this magnitude could become seismologically detectable.

Keywords: Majoritic garnet, inclusion in diamond, Brillouin scattering, pyroxenite, seismic signatures, sound velocities

INTRODUCTION


Majoritic garnet is one of the main constituents of the lowermost upper mantle and the mantle transition zone, comprising up to 35 vol% in peridotitic and up to 95 vol% in eclogitic lithologies (Wood et al. 2013). Despite having a wide stability field (~7–26 GPa) and being one of the most common minerals in Earth's mantle, the compositions of natural majoritic garnets are not very well known and there are only a few findings of

this mineral as inclusions in diamond. To date, there are only about 150 majoritic garnet inclusions in diamonds reported in the literature (Kiseeva et al. 2013) with the majority of them having either eclogitic (metabasaltic) or pyroxenitic paragenesis; observations of majoritic garnets of peridotitic paragenesis are rare and invariably relate to depleted (lithospheric mantle-like) substrates instead of pyrolite.

The compositions of majoritic garnets vary substantially. If a generic mineral formula for upper mantle garnets is described as $(\text{Mg,Ca,Fe}^{2+})_3(\text{Al,Cr,Fe}^{3+})_2(\text{SiO}_4)_3$, majoritic garnet will contain Si and Mg on the octahedral site, and in more eclogitic compositions, Na on the dodecahedral site, resulting in a more

* E-mail: kate.kiseeva@ucc.ie

† Orcid 0000-0003-0397-6511

 Open access: Article available to all readers online. This article is CC-BY.

complicated solid solution $(\text{Na}, \text{Mg}, \text{Ca}, \text{Fe}^{2+})_3(\text{Al}, \text{Cr}, \text{Fe}^{3+}, \text{Si}, \text{Mg})_2(\text{SiO}_4)_3$. Monovalent Na is charge-balanced through the coupled substitution: $\text{Na}^+ + \text{Si}^{4+} = \text{Al}^{3+} + \text{Mg}^{2+}$. In Na-poor compositions, a more divalent cation-rich (Mg, Ca, Fe^{2+}) majoritic garnet is formed, following the substitution: $\text{Si}^{4+} + \text{M}^{2+} = 2\text{Al}^{3+}$, where M^{2+} is usually Mg.

With increasing depth, the stabilization of more ferric iron-rich andradite $[\text{Ca}_3\text{Fe}_2(\text{SiO}_4)_3]$ and/or skiaegite $[\text{Fe}_3\text{Fe}_2(\text{SiO}_4)_3]$ components occur at the expense of Al-rich pyrope and almandine (Woodland and O'Neill 1993; Kiseeva et al. 2018). In their recent study on majoritic inclusions in diamond, Kiseeva et al. (2018) showed that the amount of ferric iron in majorites increases from molar $\text{Fe}^{3+}/(\text{Fe}^{3+} + \text{Fe}^{2+})$ of 0.08 at approximately 240 km depth to 0.30 at approximately 500 km depth.

The deepest majorites, derived from the transition zone, are of pyroxenitic origin (Kiseeva et al. 2013, 2016). There are several mechanisms proposed that result in the formation of pyroxenitic lithologies, one of them being through the interaction of mantle peridotite with eclogite, or eclogite-derived melts, the latter introduced into the mantle by subduction (Yaxley and Green 1998; Thomson et al. 2016). In their study on peridotite-eclogite interaction, Kiseeva et al. (2016) showed that pyroxenitic garnet will crystallize as a monomineralic layer at the reaction boundary between peridotite and a carbonated eclogite. Thomson et al. (2016) studied the products of peridotite interaction with carbonatitic melt produced by melting of carbonated subducted crust and showed that the compositions of the resulting majoritic garnets were also broadly pyroxenitic. These authors further suggested that, due to highly reducing conditions in the lowermost upper mantle and the mantle transition zone, the carbonatitic melts will also produce diamond upon reaction with ambient pyrolytic mantle (Rohrbach and Schmidt 2011). Thus, if such scenarios are common and subducting slabs indeed expel pulses of low-degree melts upon their descent into the deep mantle (e.g., Thomson et al. 2016), monomineralic lenses of garnetite and/or olivine-free pyroxenite are expected to form along the reaction fronts. At pressures exceeding the stability of pyroxenes, majoritic garnet of broadly pyroxenitic composition may be the only mineral present in the reaction zones, possibly accompanied by small amounts of stishovite or olivine/wadsleyite, depending on the bulk-rock composition (Fig. 1). Although peridotite-eclogite interaction in the presence of carbonatitic melts is a plausible scenario of pyroxenite formation in the upper mantle and the mantle transition zone, other mechanisms should not be disregarded. Hirschmann and Stolper (1996) list several processes leading to pyroxenite formation in the asthenosphere, among which subduction of oceanic crust and veined oceanic lithosphere, delamination of continental crust and subcontinental mantle, exhumation of the mantle wedge material, and metamorphic segregation. Furthermore, the authors suggest that pyroxenites may constitute 2–5% of the upper mantle, being present in the form of layers and lenses within mantle peridotites. If this material is transported to larger depths, outside of the stability field of pyroxene, the pyroxenitic layers of various compositions will be transformed into layers of pure garnetite (in compositions closer to eclogite) and garnet and olivine (in compositions closer to peridotite). Using the database of majoritic inclusions in diamonds, Kiseeva et al. (2016) recalculated the composition of parental lithology

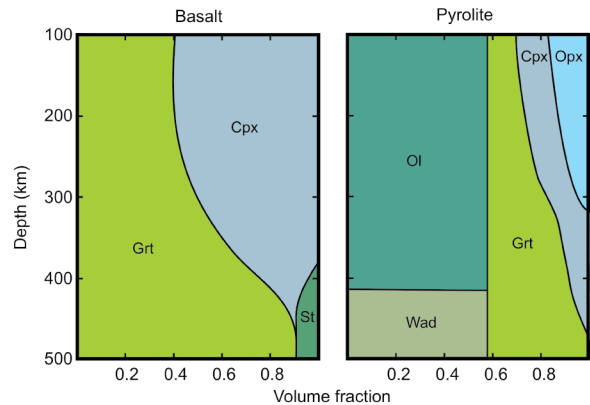


FIGURE 1. Sketch across 100–500 km depth with phase proportions in basaltic (eclogitic) and pyrolytic bulk compositions. With increasing depth, pyroxene increasingly dissolves in the garnet structure. This transition is strongly composition dependent, and the complete disappearance of clinopyroxene from the system was reported at pressures between 13 and 26 GPa. Upon clinopyroxene-out, the rocks convert to wadsleyite-majorite garnet in peridotitic assemblages or near-monomineralic garnetite (with small amounts of stishovite) in eclogitic or olivine-free pyroxenitic assemblages. Stability fields from Stixrude and Lithgow-Bertelloni (2005) and Ringwood (1991).

for ~80 majoritic inclusions, concluding that they span a wide range of intermediate compositions between typical eclogite and peridotite, from ~90% eclogite to 70% peridotite, and that most of them could have derived from monomineralic garnetite, without having been in equilibrium with a clinopyroxene. This confirms the potential for the presence of monomineralic garnetite layers in the lowermost upper mantle and transition zone. However, neither the shapes and sizes of the garnetite bodies nor their abundance in the mantle are known.

One way to enable the hypothesis of the presence of garnetite layers of pyroxenitic composition in the mantle transition zone to be tested is through an investigation of the expected seismic signature of such majoritic garnets. Because the pyroxene-garnet transition is gradual and occurs over a large pressure interval, there is no seismic discontinuity associated with the formation of majoritic garnet. However, due to its large modal abundance, majoritic garnet can have a profound effect on sound velocities and cause high velocity gradients in the transition zone (Irfune 1987).

Multiple studies on elastic properties of upper mantle garnet end-members have shown that compressional wave (V_p) and shear-wave velocities (V_s) are strongly composition-dependent and substantially differ between the garnet end-members ($V_s = 4.6\text{--}5.5$ km/s and $V_p = 8.3\text{--}9.3$ km/s) (Wang and Ji 2001). It is, however, not well known how variations in composition affect sound velocities of majoritic garnet (Irfune et al. 2008). There are only a few studies of elastic properties of majoritic garnets, with most of them being conducted on synthetic samples, investigating either end-members or relatively simple solid-solutions (e.g., Sinogeikin and Bass 2002; Irfune et al. 2008; Murakami et al. 2008; Pamato et al. 2016; Vasiukov et al. 2018; Liu et al. 2019; Sanchez-Valle et al. 2019). The scarcity of sound wave velocity data on natural majorites is due to the rarity of samples

TABLE 1. Normalized molar fractions of studied majoritic inclusions in diamonds

	Pyrope $\text{Mg}_3\text{Al}_2(\text{SiO}_4)_3$	Andradite $\text{Ca}_3\text{Fe}_2(\text{SiO}_4)_3$	Na-majorite $\text{Na}_2\text{MgSi}_3\text{O}_{12}$	Almandine $\text{Fe}_3\text{Al}_2(\text{SiO}_4)_3$	Mg-Majorite $\text{Mg}_3(\text{MgSi})(\text{SiO}_4)_3$	Grossular $\text{Ca}_3\text{Al}_2(\text{SiO}_4)_3$
37b	0.524	0.047	0.010	0.230	0.062	0.120
39a	0.379	0.066	0.026	0.177	0.264	0.082
55a	0.265	0.084	0.030	0.130	0.381	0.104

Notes: For chemical composition in wt% oxides, see Supplemental¹ Table S1. For simplicity, Na-majorite was omitted from sound velocity calculations with the sums normalized to 100%. Based on EPMA data, uncertainties on the values are no higher than 5%

and very small crystal sizes (<200 μm).

To date, elasticity measurements of natural majorites were only obtained on Mg-rich polycrystalline samples from the Catherwood meteorite, with no data being available for natural single-crystal majorites (Kavner et al. 2000; Sinogeikin and Bass 2002).

Given the role of majoritic garnet as a rock-forming mineral in the Earth's mantle at depths of ~300–750 km, and as a key host for a wide array of both compatible and incompatible elements, the purpose of this study is to determine the elastic properties of natural single-crystal majoritic garnets and to test whether garnetite layers, formed as a result of the pyroxenite–garnetite transformation at the pressures of the mantle transition zone could be seismically detectable.

MATERIALS AND METHODS

Samples

For this study, we selected three natural single-crystal majoritic garnet inclusions in diamonds (37B, 39A, and 55A) from the Jagersfontein kimberlite in South Africa (Supplemental¹ Table S1 and Table 1). The inclusions were about 100–200 μm in size and optically transparent (Fig. 2 and optical images in Kiseeva et al. 2018). For previous studies, the inclusions were separated from the host diamond, mounted in epoxy disks with 0.7 mm thickness supported by brass rings and then polished on one side. For Brillouin scattering measurements, the crystals were released from the initial epoxy and polished on both sides to a thickness of 50–30 μm .

The crystals were previously analyzed by electron microprobe for major element compositions (Tappert et al. 2005), by X-ray diffraction (XRD) for structure, and by synchrotron Mössbauer source (SMS) spectroscopy (beamline ID18 at the European Synchrotron Radiation Facility, Grenoble) for ferric-ferrous ratios (Kiseeva et al. 2018). The XRD analysis conducted at beamline P02 at PETRA III, Hamburg, confirmed the majorites as monophase single crystals (Kiseeva et al. 2018). Major element compositions, ferric-ferrous ratios and garnet components

of the studied majorites are summarized in Table 1 and Supplemental¹ Table S1.

The studied majoritic garnets are of pyroxenitic composition and contain relatively high concentrations of CaO (5.7–7.3 wt%), but low Cr_2O_3 (0.13–0.36) with up to 0.1–0.4 wt% Na_2O and intermediate Mg# (0.70–0.81). Their ferric iron content is 12–30% of total iron, as opposed to 5–10% in the typical upper mantle garnets (Canil and O'Neill 1996; Kiseeva et al. 2018). More details about these inclusions and their host diamonds can be found in Tappert et al. (2005) and Kiseeva et al. (2018). The pressure of the last equilibration of these majorites was determined using the geobarometer of Beyer and Frost (2017) (Supplemental¹ Table S1). This geobarometer is based on experimentally synthesized garnet-clinopyroxene pairs. However, given that the studied inclusions are single grains (no coexisting clinopyroxene inclusions), all clinopyroxene in the source regions may have already completely dissolved in garnet, rendering the calculated pressures minimum pressures (Beyer and Frost 2017).

The origins of these inclusions were previously addressed by studies of their oxygen isotope composition (Ickert et al. 2015) and the carbon isotope composition of their enclosing diamond (Tappert et al. 2005). These isotopic signatures suggest a subduction origin, which indicates that the studied majoritic garnets could be plausible candidates to have formed through the pyrolyte–metabasalt interaction mechanism. Formation through the reaction of slab-derived carbonatitic melts and ambient mantle is supported by elevated amounts of ferric iron in majorite, possibly produced as oxidation of Fe^{2+} into Fe^{3+} upon reduction of carbon from carbonate into diamond (Kiseeva et al. 2018).

Brillouin scattering

Elastic wave velocities were measured in forward symmetric scattering geometry (Whitfield et al. 1976; Speziale et al. 2014) using the Brillouin system at BGI Bayreuth. The wavelength of the (Nd:YVO₄) laser light was 532 nm. The power of the incident beam measured before the sample was 30–60 mW. A multipath tandem Fabry–Perot interferometer (Lindsay et al. 1981) was used to solve Brillouin frequency shifts, and a single photon counting module was employed for signal detection, respectively.

Although uncertainties on measurements derived from signal-to-noise ratio are in general less than 1% (Table 2), due to the small size of the crystals and high risk of sample loss during sample preparation, the polished surfaces were relatively small in comparison to the thickness of the crystals. This causes occasional deviations from the perfect platelet scattering geometry that is required for Brillouin spectroscopy.

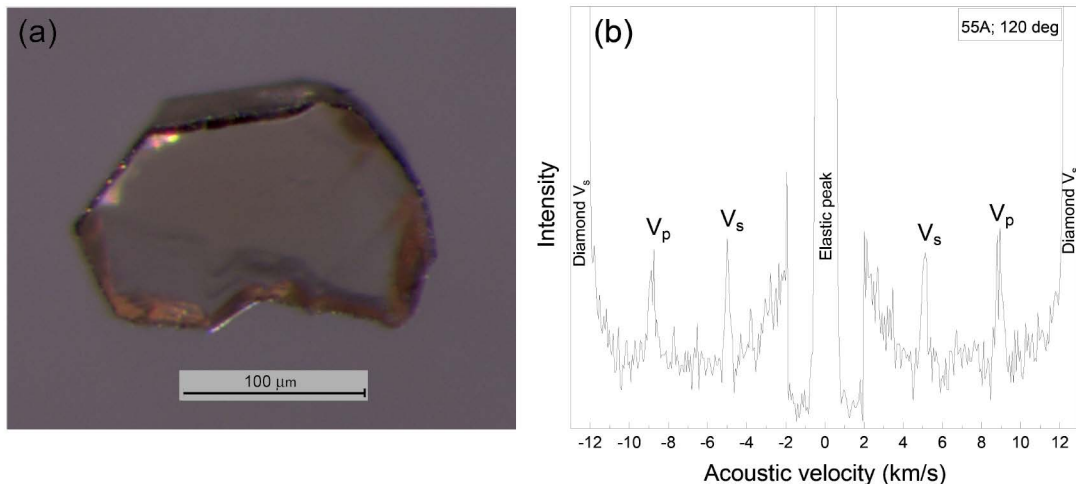


FIGURE 2. (a) Optical microscope image of inclusion JF-55A, (b) Typical Brillouin spectrum of sample JF 55a.

TABLE 2. Measured acoustic wave velocities as function of rotation angle

37b			39a			55a		
Angle (°)	V_s (km/s)	V_p (km/s)	Angle (°)	V_s (km/s)	V_p (km/s)	Angle (°)	V_s (km/s)	V_p (km/s)
0	5.144(38)	8.776(14)	0	4.962(8)	8.771(7)	0	4.985(3)	8.849(9)
20	5.079(10)	8.653(11)	20	4.967(6)	8.746(7)	20	5.127(3)	8.985(8)
40	5.017(5)	8.863(8)	40	4.944(4)	8.751(8)	40	5.166(3)	9.108(8)
60	5.045(32)	8.898(33)	60	4.951(12)	8.779(19)	80	5.095(3)	9.069(11)
70	5.044(6)	8.928(8)	80	4.921(21)	8.781(8)	120	5.07(21)	8.953(33)
80	4.999(3)	8.895(8)	100	4.929(7)	8.692(14)	140	5.046(21)	8.926(33)
100	5.000(6)	8.846(14)	120	4.930(9)	8.711(15)	160	4.926(4)	8.825(11)
120	5.066(10)	8.921(14)	140	4.905(2)	8.755(6)	180	4.908(11)	8.742(21)
140	5.017(5)	8.827(8)	160	4.881(2)	8.711(8)	-10	5.010(4)	8.937(14)
180	4.979(6)	8.836(14)	-10	4.979(2)	8.816(10)	-30	4.940(3)	8.809(8)
-10	5.007(8)	8.743(14)	-30	4.987(2)	8.869(2)	-50	4.896(3)	8.626(8)
-30	5.044(4)	8.687(4)	-50	5.010(8)	8.860(22)	-70	4.843(14)	8.596(17)
-50	5.017(3)	8.813(3)	-70	5.011(6)	8.816(2)	-90	4.811(14)	8.502(21)
-70	4.972(5)	8.808(11)	-90	4.987(2)	8.830(11)	Average	4.986	8.841
-90	4.941(33)	8.813(33)	-110	4.957(2)	8.802(5)	St.dev./n ^{1/2}	0.031	0.051
-110	4.947(14)	8.781(21)	-130	4.949(2)	8.799(3)			
-130	4.968(5)	8.746(8)	-150	4.932(3)	8.725(4)			
-150	4.958(3)	8.750(5)	-170	4.935(2)	8.715(3)			
-170	4.960(61)	8.731(61)	-180	4.928(2)	8.711(10)			
Average	5.011	8.806	Average	4.951	8.771			
St.dev./n ^{1/2}	0.012	0.018	St.dev./n ^{1/2}	0.008	0.012			

Notes: The uncertainty of individual measurements at specific chi angles was estimated from signal-to-noise ratio following Kurnosov et al. (2017) and is lower than 1% (values in parentheses). Due to imperfect sample polishment, data are scattered and therefore aggregate velocity is estimated as an average with standard error (see text for discussion, Supplemental¹ Fig. S1).

copy measurements (Whitfield et al. 1976; Speziale et al. 2014) and may explain the scatter seen in the obtained sound velocities (Table 2, Supplemental¹ Fig. S1).

Considering that the scatter appears random, and garnets generally show weak elastic anisotropy (Murakami et al. 2008), we assume that the variation of measured velocities with direction is caused by the deviation from ideal platelet geometry rather than an intrinsic elastic anisotropy (which should follow a more systematic trend).

To compromise between data quality and sample preservation, we used the least possible and safe polishing and compensated it with multiple (13–19) measurements along 360° range of directions. Therefore, Brillouin measurements were performed in different crystallographic directions by rotating the sample within the scattering plane. Measurements were taken with a step size of about 20° over a large range of angles, covering almost the full 360° angular range.

The aggregate velocities and elastic moduli were obtained by averaging acoustic velocities over several crystallographic directions (e.g., Sinogeikin and Bass 2000) and uncertainty was estimated as standard error (Table 2, Supplemental¹ Fig. S1). The resulting uncertainty values deviate from the average more than it is suggested from estimations based on the signal-to-noise ratio. That is why the standard deviation from all measurements was used as an upper limit of uncertainty estimation. In the case of samples 37b and 39a, it did not exceed 1%. For sample 55a, the measured sound velocities have a standard deviation of ~2%. We provide standard errors as a measure of uncertainty on figures and tables in the main text.

RESULTS AND DISCUSSION

Ferric iron in natural majorites and its effect on sound velocities

It has been observed that ferric iron in majoritic garnets increases with pressure (Kiseeva et al. 2018). XRD diffraction patterns of the studied majorites provide estimates of the site occupancy of different elements. Given their complex chemical composition and relatively large amounts (up to 3 wt%) of minor and trace elements (Na₂O, MnO, Cr₂O₃, TiO₂, rare earth elements), it is impossible to precisely evaluate the occupancy of X and Y sites. Ferric iron on the Y-site can be present as one of three components: andradite [Ca₃Fe₂(SiO₄)₃], khoharite [Mg₃Fe₂(SiO₄)₃], or skiaquite [Fe₃Fe₂(SiO₄)₃] among which only andradite is common in nature and its elastic properties are very well-studied. As the choice of end-members for recalculation of garnet into individual components does not affect sound

velocities (Vasiukov et al. 2018), for simplicity, we assume that all ferric iron is present in the andradite component. The andradite component in the studied garnets is relatively small and varies between 4.6 and 8.3 mol% (Table 1).

Figure 3 shows the relationship of sound velocities, measured at ambient conditions, with the pressure of the last equilibration. There appear to be no correlations among velocity, pressure of formation, and ferric iron content. This is consistent with our estimate that ferric iron ratios of 30% in our deepest samples will translate to ~8% andradite component only (Table 1, Supplemental¹ Table S1). Due to the small differences in sound velocities with almandine and pyrope, such a small andradite component will not be detectable by seismic measurements.

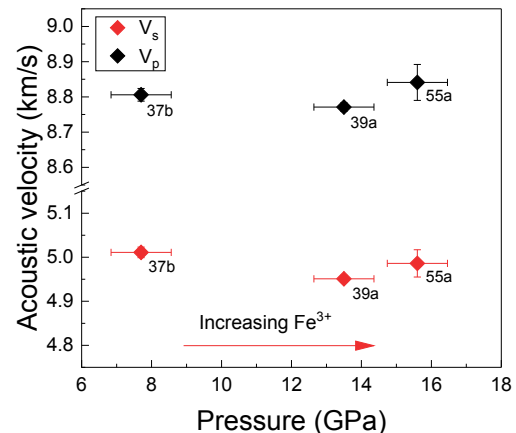


FIGURE 3. Sound velocity as a function of the pressure of last equilibration estimated from garnet compositions (Beyer and Frost 2017). The relative percentage of ferric iron ($100 \cdot \text{Fe}^{3+}/\text{Fe}_{\text{tot}}$) for the studied majoritic garnets is 12% for 37b, 20% for 39a, and 30% for 55a. Error bars for sound velocities are standard errors (Table 2).

TABLE 3. Literature data for elastic parameters of individual garnet end-members (Jiang et al. 2004; Kono et al. 2010; Arimoto et al. 2015; Chantel et al. 2016; Liu et al. 2019)

	Chantel et al. 2016 Pyrope Mg ₃ Al ₂ (SiO ₄) ₃	Jiang et al. 2004 Andradite Ca ₃ Fe ₂ (SiO ₄) ₃	Arimoto et al. 2015 Almandine Fe ₃ Al ₂ (SiO ₄) ₃	Liu et al. 2019 Majorite Mg ₃ (MgSi)(SiO ₄) ₃	Kono et al. 2010 Grossular Ca ₃ Al ₂ (SiO ₄) ₃
K ₀ (GPa)	172.0(16)	154.5(6)	172.6(11)	158(2)	171.5(8)
G ₀ (GPa)	89.1(5)	89.7(4)	94.2(3)	83(1)	108.4(3)
ρ (g/cm ³)	3.565(5)	3.843(5)	4.3188(2)	3.518(6)	3.599(6) ^a

Notes: Numbers in parentheses indicate standard deviation used in this study.

^a Density estimation is based on reported data points, which were fitted with second-order Birch-Murnaghan equation of state.

Sound velocities of end-members and solid solutions

Over the last decades, the elastic properties of upper mantle garnet end-members have been relatively well-investigated at physical conditions relevant for the Earth's interior, and are generally consistent with each other (Wang and Ji 2001). The complexity of natural garnet chemical composition necessitates the ability to transfer the elastic properties of individual end-members to solid solutions (e.g., Chantel et al. 2016; Pamato et al. 2016). At ambient conditions, it has been shown that the elastic properties of the members of the pyrospite garnet series (pyrope-almandine-spessartine) are linearly dependent on the properties of the end-members (Erba et al. 2014).

In this study, we compared the measured sound velocities for the natural majoritic garnets with the sound velocities calculated from individual end-members. We calculated physical parameters (A), i.e., density and elastic moduli of our majoritic garnets as $A = \sum_{i=1}^N m_i A_i$. This approach involves the use of the molar end-member fraction (m_i) and physical parameters of the i -th constituent (A_i), which are listed in Tables 1 and 3, respectively. We then use the calculated physical parameters to determine

$$V_p = \sqrt{\frac{K + 4G/3}{\rho}}$$

and

$$V_s = \sqrt{\frac{G}{\rho}}$$

where K is the bulk modulus, G is the shear modulus and ρ is the density. The measured and calculated sound velocities are in good agreement (Supplemental¹ Table S2). This suggests that, at least at ambient conditions, the linear relationship between solid solutions and end-members observed for the upper mantle garnets can be extrapolated to majoritic garnets from the mantle transition zone.

Some experimental data exist on the elasticity of majoritic garnets at high pressure and high temperature (Pamato et al. 2016; Irifune et al. 2008), but the available data do not allow for a comprehensive evaluation of the effects of chemical variabilities on elasticity. The here-presented calculations are, therefore, performed for ambient conditions. The results can serve to guide future work but might need revision once more comprehensive data on the elasticity of majoritic garnets at conditions of the upper mantle become available. We note that few studies suggest more complicated mixing behaviors at high pressure and high temperature. For example, the elasticity of pyrospite garnets shows a more complicated behavior that cannot be approximated with a linear function (Du et al. 2015).

IMPLICATIONS FOR THE SEISMIC DETECTION OF PYROXENITE IN THE DEEP UPPER MANTLE

As confirmed by our measurements on natural majoritic garnets from the deep upper mantle and transition zone, majorite shows the highest elastic wave velocities among all major upper mantle phases. This opens the possibility that pyroxenitic or monomineralic garnet layers lead to a detectable seismic signature if they occur on length scales comparable to or larger than the seismic wavelength. Here, we use our results derived from natural deep mantle majorities to evaluate the possible seismic signal of majorite-rich regions. In particular, we modeled the seismic contrasts for a mineral assemblage expected at eclogite-pyroxenite and peridotite-pyroxenite interfaces at 350 km.

For the purpose of our model, we considered a scenario with eclogitic rocks being in contact with the average peridotitic mantle (Fig. 4a). At the formation conditions of our garnet 39a (~13 GPa, 350 km depth), standard peridotitic mantle consists of 56 vol% of olivine, 10 vol% of pyroxene, and 34 vol% of garnet (Frost 2008). At the same depth, subducted eclogitic rocks are expected to have a volumetric abundance of majoritic garnets of 65% while the remaining fraction is occupied by pyroxenes and a negligible fraction of stishovite (Irifune et al. 1986). The elastic moduli K and G of these polymineralic isotropic aggregates (rocks) can be evaluated by averaging Voigt (M_V) and Reuss (M_R) bounds, which are formulated as $M_V = \sum_{i=1}^N M_i f_i$ and $1/M_R = \sum_{i=1}^N f_i / M_i$ where N is the number of different minerals in the aggregate, f_i and M_i are the volume fractions and elastic moduli of the i -th constituent (Avseth et al. 2010).

Isotropic velocities of the minerals considered in our modeling are listed in Supplemental¹ Table S2, while assumed volume fractions are reported in Supplemental¹ Table S3. Since the here-reported measurements were performed at room conditions only, we do not have any constraints on the pressure- and temperature-dependency of the elastic properties of our samples. Therefore, we restrict our calculations to ambient conditions. Our modeling, however, accounts for variations of stable mineral assemblages with depth. The chemical composition and, as a consequence, the elastic properties, assumed for the modeled garnets reflect their geological context. Peridotitic garnets have a higher Mg# [molar Mg/(Mg+Fe), usually >0.8], and contain relatively small amounts of Ca (up to 4–5 wt% CaO) and very high amounts of Cr (up to 20–25 wt% Cr₂O₃) when compared to eclogitic garnets that contain <1 wt% Cr₂O₃ and up to 20 wt% CaO (Sobolev et al. 1973). Calcium, chromium, and Mg# are the main discriminators between the two types of garnets, however, in addition to these, garnet compositions also differ in the concentrations of Ti, with eclogitic garnets containing up to a few percent TiO₂.

Pyroxenitic garnet is intermediate in its composition between peridotitic and eclogitic garnets, and usually exhibits interme-

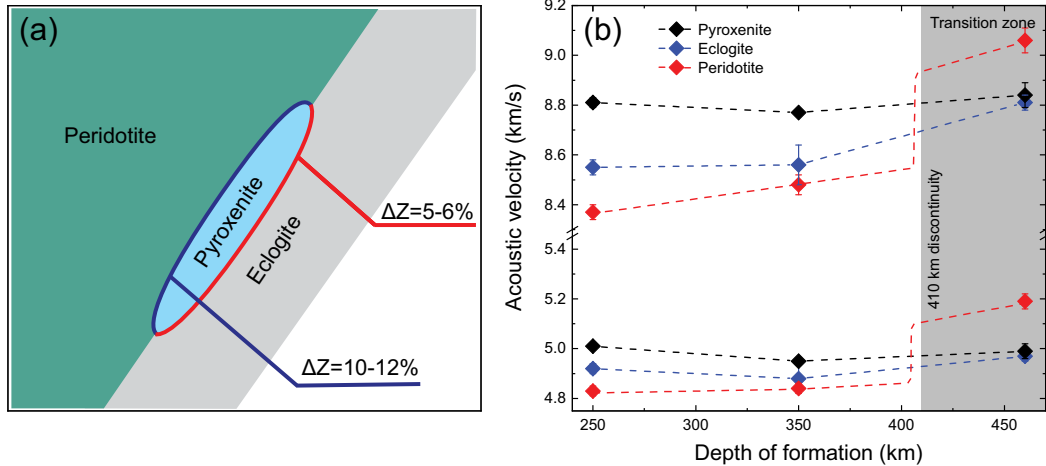


FIGURE 4. Illustration of the seismic velocity and impedance contrasts expected in a scenario where a pyroxenitic majorite layer forms through the reaction of peridotite/pyrolite with eclogite/metabasalt. (a) Cartoon to illustrate the formation of a pyroxenitic majorite layer at the interface between eclogite and peridotite. The modeled seismic impedance contrasts at the boundaries between peridotite and pyroxenite (red) and pyroxenite and eclogite (orange) are given in the figure. Modeling has been done for typical mantle assemblages expected at 350 km (median depth of origin of our majorite inclusions), but using elastic properties and densities at ambient conditions. (b) Compressional and shear wave velocities of the three natural majoritic garnets measured in this study (black solid diamonds) in comparison to the expected seismic velocities for peridotite/pyrolite (green diamonds) and eclogite/metabasalt (blue diamonds). “Depth of formation” in **b** refers to the depths at which the here-studied garnets likely formed in Earth’s mantle. The seismic wave velocities of peridotite/pyrolite and eclogite/metabasalt were calculated using ambient conditions elastic properties, but employing a mineralogy expected at the respective depths. See text for more details.

diate CaO concentrations, low Cr-concentrations (similar but slightly higher than eclogitic garnet), but lower Ti and high Mg#, more characteristic of peridotitic garnets (Kiseeva et al. 2013, 2016).

As a result, the pyrope, grossular, almandine, and Cr-bearing knorringite/uvarovite components significantly differ for the three types of garnet. Peridotitic garnets contain a significantly larger proportion of pyrope $[\text{Mg}_3\text{Al}_2(\text{SiO}_4)_3]$ and uvarovite $[\text{Ca}_3\text{Cr}_2(\text{SiO}_4)_3]$ components and are poorer than eclogitic garnets in grossular $[\text{Ca}_3\text{Al}_2(\text{SiO}_4)_3]$ and almandine $[\text{Fe}_3\text{Al}_2(\text{SiO}_4)_3]$ components. Pyroxenitic garnets are high in pyrope and low in uvarovite.

Our results only serve as an indication of whether pyroxenite could be detectable by seismology. Resulting physical properties of the modeled mantle rocks are listed in Table 4. As expected, we found that both P- and S-waves propagate faster

in pyroxenite than in both bulk-rock peridotite and eclogite at ambient conditions. Compared to peridotite, V_p and V_s in our pyroxenitic garnets are expected to be faster by 3.3(5)% and 1.9(6)%, respectively. This is because 66 vol% of a peridotite consists of olivine and clinopyroxene at 350 km depth. In these two minerals, seismic waves propagate at lower velocities than in peridotitic garnet, which constitutes the remaining volume of the bulk rock. Given a large enough thickness of the possible pyroxenitic garnetite layer, velocity differences to ambient peridotitic mantle are expected to be seismologically detectable (Wit et al. 2012). When olivine transforms to wadsleyite at approximately 410 km depths, the situation changes in that pyrolite will become seismically faster by about 2.3(8)% in V_p and 3.8(8)% in V_s than pyroxenite.

Similarly, the velocity contrast between eclogite/metabasalt and pyroxenite ranges from 1.3(13)% in S-wave velocities to 2.4(10)% in P-wave velocities. Unlike peridotitic garnet, eclogitic garnet has similar V_p and V_s as pyroxenitic garnet because of its high Fe content (28 mol% almandine), which lowers propagation velocities of both P- and S-waves. Therefore, the velocity contrast is only due to the presence of seismically slow Ca-clinopyroxene in the eclogitic rock. The seismic reflection coefficient, however, does not depend on the velocity contrasts alone but is sensitive to the impedance contrast across an interface. Pyroxenite is denser than eclogite but also has higher bulk and shear moduli, which make it seismically faster. The impedance contrast across a possible pyroxenite-eclogite interface amounts to almost 6% for V_p and 5% for V_s , which might be strong enough for detection by seismology. The impedance contrast across a pyroxenite-peridotite interface for the mineral assemblage expected at 350 km depth is much higher and calculated to be about 12% (V_p) and 10% (V_s). The impedance

TABLE 4. Physical parameters and acoustic velocities of pyroxenitic, peridotitic, and eclogitic mantle rocks calculated at ambient conditions, but employing the mineralogy expected at the pressure of formation P_{form} of the here-measured garnets (also see Supplemental Table S3)

$P_{\text{form}} = 8 \text{ GPa}$	$\rho \text{ (g/cm}^3\text{)}$	$K_{\text{VRH}} \text{ (GPa)}$	$G_{\text{VRH}} \text{ (GPa)}$	$V_p \text{ (km/s)}$	$V_s \text{ (km/s)}$
Pyroxenite	3.774(5)	167(1)	94.6(5)	8.81(2)	5.01(1)
Peridotite	3.418(2)	133(2)	79.8(7)	8.37(3)	4.83(2)
Eclogite	3.468(2)	142.0(14)	84(1)	8.55(3)	4.92(2)
$P_{\text{form}} = 13 \text{ GPa}$					
Pyroxenite	3.738(5)	165(1)	91.5(5)	8.77(1)	4.95(1)
Peridotite	3.455(2)	140(2)	81(1)	8.48(4)	4.85(2)
Eclogite	3.620(3)	150(4)	86(2)	8.56(8)	4.88(6)
$P_{\text{form}} = 16 \text{ GPa}$					
Pyroxenite	3.701(5)	166(3)	92.2(10)	8.84(5)	4.99(3)
Peridotite	3.615(8)	167(2)	97(1)	9.06(5)	5.19(3)
Eclogite	3.719(4)	166(3)	92(1)	8.81(3)	4.97(2)

contrast between pyroxenite and eclogite is expected to be strongly depth-dependent since it is sensitive to the pyroxene/garnet ratio in eclogite.

Based on our modeling, a monomineralic majoritic garnet layer of sufficient size will be seismically faster, about 3% for V_p and 2% for V_s , than both peridotite and eclogite above the transition zone, with the exact values being a function of depth. In the transition zone, the situation becomes more complicated with pyrolite becoming seismically faster than majorite-garnetite, due to the olivine-wadsleyite transition (Fig. 4). Throughout the transition zone sound velocities are increasing, with a sharp rise being observed at the transition zone lower mantle boundary. The composition of the rocks in that region remains debated (e.g., Irifune et al. 2008), with several recent studies suggesting an enrichment in basaltic lithologies throughout the mantle transition zone (Ballmer et al. 2015) and at the transition zone lower mantle boundary (Greaux et al. 2019). These findings are in good agreement with the possible presence of pyroxenites in the deeper regions of the Earth.

Although our measurements and modeling were performed at ambient conditions, these first results indicate that pyroxenite layers, predicted to exist at the interface of subducting slabs and ambient convecting mantle, could be detected seismologically at depth shallower than 410 km. Future experiments and modeling at elevated pressure and temperature conditions are, however, required to put tighter quantitative constraints on the seismic signature of pyroxenite in the deep mantle.

ACKNOWLEDGMENTS

We thank Johannes Buchen for providing wadsleyite elasticity data. We also thank Denis Vasiukov for comments and discussion. Many thanks to two anonymous reviewers for their valuable comments that significantly improved this manuscript and a special thank you to Fabrizio Nestola for editorial handling.

FUNDING

This research was supported through the project “GeoMaX” funded under the Emmy-Noether Program of the German Foundation DFG (MA4534/3-1). H.M. acknowledges support from the Bavarian Academy of Sciences. E.S.K. was supported by NERC grant NE/L010828/1. N.S. was supported by the IRTG “Deep Earth Volatile Cycles” grant (GRK 2156/1).

REFERENCES CITED

- Arimoto, T., Greaux, S., Irifune, T., Zhou, C.Y., and Higo, Y. (2015) Sound velocities of $\text{Fe}_3\text{Al}_2\text{Si}_5\text{O}_{12}$ almandine up to 19 GPa and 1700 K. *Physics of the Earth and Planetary Interiors*, 246, 1–8.
- Avseth, P., Mukerji, T., Mavko, G., and Dvorkin, J. (2010) Rock-physics diagnostics of depositional texture, diagenetic alterations, and reservoir heterogeneity in high-porosity siliciclastic sediments and rocks—A review of selected models and suggested work flows. *Geophysics*, 75, A31–A47.
- Ballmer, M.D., Schmerr, N.C., Nakagawa, T., and Ritsema, J. (2015) Compositional mantle layering revealed by slab stagnation at similar to 1000 km depth. *Science Advances*, 1, 11.
- Beyer, C., and Frost, D.J. (2017) The depth of sub-lithospheric diamond formation and the redistribution of carbon in the deep mantle. *Earth and Planetary Science Letters*, 461, 30–39.
- Chantel, J., Manthilake, G.M., Frost, D.J., Beyer, C., Boffa Ballaran, T., Jing, Z.C., and Wang, Y.B. (2016) Elastic wave velocities in polycrystalline $\text{Mg}_3\text{Al}_2\text{Si}_5\text{O}_{12}$ -pyrope garnet to 24 GPa and 1300 K. *American Mineralogist*, 101, 991–997.
- Canil, D., and O'Neill, H.St.C. (1996) Distribution of ferric iron in some upper-mantle assemblages. *Journal of Petrology*, 37, 609–635.
- Du, W., Clark, S.M., and Walker, D. (2015) Thermo-compression of pyrope-grossular garnet solid solutions: Non-linear compositional dependence. *American Mineralogist*, 100, 215–222.
- Erba, A., Mahmoud, A., Orlando, R., and Dovesi, R. (2014) Elastic properties of six silicate garnet end members from accurate ab initio simulations. *Physics and Chemistry of Minerals*, 41, 151–160.
- Frost, D.J. (2008) The upper mantle and transition zone. *Elements*, 4, 171–176.
- Greaux, S., Irifune, T., Higo, Y., Tange, Y., Arimoto, T., Liu, Z.D., and Yamada, A. (2019) Sound velocity of CaSiO_3 perovskite suggests the presence of basaltic crust in the Earth's lower mantle. *Nature*, 565, 218–221.
- Hirschmann, M.M., and Stolper, E.M. (1996) A possible role for garnet pyroxenite in the origin of the “garnet signature” in MORB. *Contributions to Mineralogy and Petrology*, 124, 185–208.
- Ickert, R.B., Stachel, T., Stern, R.A., and Harris, J.W. (2015) Extreme ^{18}O -enrichment in majorite constrains a crustal origin of transition zone diamonds. *Geochemical Perspectives Letters*, 1, 65–74.
- Irifune, T. (1987) An experimental investigation of the pyroxene garnet transformation in a pyrolite composition and its bearing on the constitution of the mantle. *Physics of the Earth and Planetary Interiors*, 45, 324–336.
- Irifune, T., Sekine, T., Ringwood, A.E., and Hibberson, W.O. (1986) The eclogite-garnetite transformation at high-pressure and some geophysical implications. *Earth and Planetary Science Letters*, 77, 245–256.
- Irifune, T., Higo, Y., Inoue, T., Kono, Y., Ohfuji, H., and Funakoshi, K. (2008) Sound velocities of majorite garnet and the composition of the mantle transition region. *Nature*, 451, 814–817.
- Jiang, F.M., Speziale, S., Shieh, S.R., and Duffy, T.S. (2004) Single-crystal elasticity of andradite garnet to 11 GPa. *Journal of Physics: Condensed Matter*, 16, S1041–S1052.
- Kavner, A., Sinogeikin, S.V., Jeanloz, R., and Bass, J.D. (2000) Equation of state and strength of natural majorite. *Journal of Geophysical Research: Solid Earth*, 105, 5963–5971.
- Kiseeva, E.S., Yaxley, G.M., Stepanov, A.S., Tkalcic, H., Litasov, K.D., and Kamenetsky, V.S. (2013) Metapyroxenite in the mantle transition zone revealed from majorite inclusions in diamonds. *Geology*, 41, 883–886.
- Kiseeva, E.S., Wood, B.J., Ghosh, S., and Stachel, T. (2016) The pyroxenite-diamond connection. *Geochemical Perspectives Letters*, 2, 1–9.
- Kiseeva, E.S., Vasiukov, D.M., Wood, B.J., McCammon, C., Stachel, T., Bykov, M., Bykova, E., Chumakov, A., Cerantola, V., Harris, J.W., and Dubrovinsky, L. (2018) Oxidized iron in garnets from the mantle transition zone. *Nature Geoscience*, 11, 144–150.
- Kono, Y., Greaux, S., Higo, Y., Ohfuji, H., and Irifune, T. (2010) Pressure and temperature dependences of elastic properties of grossular garnet up to 17 GPa and 1650 K. *Journal of Earth Science*, 21, 782–791.
- Kurnosov, A., Marquardt, H., Frost, D.J., Boffa Ballaran, T., and Ziberna, L. (2017) Evidence for a Fe^{3+} -rich pyrolytic lower mantle from (Al,Fe)-bearing bridgmanite elasticity data. *Nature*, 543, 543–548.
- Lindsay, S.M., Anderson, M.W., and Sandercock, J.R. (1981) Construction and alignment of a high performance multipass vernier tandem Fabry-Perot interferometer. *Review of Scientific Instruments*, 52(10), 1478–1486.
- Liu, Z.D., Greaux, S., Cai, N., Siersch, N., Boffa Ballaran, T., Irifune, T., and Frost, D.J. (2019) Influence of aluminum on the elasticity of majorite-pyrope garnets. *American Mineralogist*, 104, 929–935.
- Murakami, M., Sinogeikin, S.V., Litasov, K., Ohtani, E., and Bass, J.D. (2008) Single-crystal elasticity of iron-bearing majorite to 26 GPa: Implications for seismic velocity structure of the mantle transition zone. *Earth and Planetary Science Letters*, 274, 339–345.
- Pamato, M.G., Kurnosov, A., Boffa Ballaran, T., Frost, D.J., Ziberna, L., Giannini, M., Speziale, S., Tkachev, S.N., Zhuravlev, K.K., and Prakupenka, V.B. (2016) Single crystal elasticity of majoritic garnets: Stagnant slabs and thermal anomalies at the base of the transition zone. *Earth and Planetary Science Letters*, 451, 114–124.
- Ringwood, A.E. (1991) Phase transformations and their bearing on the constitution and dynamics of the mantle. *Geochimica et Cosmochimica Acta*, 55, 2083–2110.
- Rohrbach, A., and Schmidt, M.W. (2011) Redox freezing and melting in the Earth's deep mantle resulting from carbon-iron redox coupling. *Nature*, 472, 209–212.
- Sinogeikin, S.V., and Bass, J.D. (2000) Single-crystal elasticity of pyrope and MgO to 20 GPa by Brillouin scattering in the diamond cell. *Physics of the Earth and Planetary Interiors*, 120, 43–62.
- Sanchez-Valle, C., Wang, J.Y., and Rohrbach, A. (2019) Effect of calcium on the elasticity of majoritic garnets and the seismic gradients in the mantle transition zone. *Physics of the Earth and Planetary Interiors*, 293, 1–5.
- Sinogeikin, S.V., and Bass, J.D. (2002) Elasticity of pyrope and majorite-pyrope solid solutions to high temperatures. *Earth and Planetary Science Letters*, 203, 549–555.
- Sobolev, N.V., Lavrent'ev, Y.G., Pokhilenko, N.P., and Usova, L.V. (1973) Chrome-rich garnets from kimberlites of Yakutia and their parageneses. *Contributions to Mineralogy and Petrology*, 40, 39–52.
- Speziale, S., Marquardt, H., and Duffy, T.S. (2014) Brillouin scattering and its application in geosciences. *Spectroscopic Methods in Mineralogy and Materials Science*, 78, 543–603.
- Stixrude, L., and Lithgow-Bertelloni, C. (2005) Thermodynamics of mantle minerals—I. Physical properties. *Geophysical Journal International*, 162, 610–632.
- Tappert, R., Stachel, T., Harris, J.W., Muehlenbachs, K., Ludwig, T., and Brey, G.P. (2005) Subducting oceanic crust: The source of deep diamonds. *Geol-*

- ogy, 33, 565–568.
- Thomson, A.R., Walter, M.J., Kohn, S.C., and Brooker, R.A. (2016) Slab melting as a barrier to deep carbon subduction. *Nature*, 529, 76–79.
- Vasiukov, D.M., Ismailova, L., Kuppenko, I., Cerantola, V., Sinmyo, R., Glazyrin, K., McCammon, C., Chumakov, A.I., Dubrovinsky, L., and Dubrovinskaia, N. (2018) Sound velocities of skiaigite–iron–majorite solid solution to 56 GPa probed by nuclear inelastic scattering. *Physics and Chemistry of Minerals*, 45, 397–404.
- Wang, Z.C., and Ji, S.C. (2001) Elasticity of six polycrystalline silicate garnets at pressure up to 3.0 GPa. *American Mineralogist*, 86, 1209–1218.
- Whitfield, C.H., Brody, E.M., and Bassett, W.A. (1976) Elastic moduli of NaCl by Brillouin scattering at high pressure in a diamond anvil cell. *Review of Scientific Instruments*, 47(8), 942–947.
- Wit, R.W.L., Trampert, J., and Hilst, R.D. (2012) Toward quantifying uncertainty in travel time tomography using the null-space shuttle. *Journal of Geophysical Research: Solid Earth*, 117 (B3).
- Wood, B.J., Kiseeva, E.S., and Matzen, A.K. (2013) Garnet in the Earth’s mantle. *Elements*, 9, 421–426.
- Woodland, A.B., and O’Neill, H.St.C. (1993) Synthesis and stability of $\text{Fe}_3^{2+}\text{Fe}_2^{3+}\text{Si}_3\text{O}_{12}$ garnet and phase relations with $\text{Fe}_2\text{Al}_2\text{Si}_3\text{O}_{12}$ – $\text{Fe}_3^{2+}\text{Fe}_2^{3+}\text{Si}_3\text{O}_{12}$ solutions. *American Mineralogist*, 78, 1002–1015.
- Yaxley, G.M., and Green, D.H. (1998) Reactions between eclogite and peridotite: mantle refertilisation by subduction of oceanic crust. *Schweizerische Mineralogische Und Petrographische Mitteilungen*, 78, 243–255.

MANUSCRIPT RECEIVED MAY 29, 2019

MANUSCRIPT ACCEPTED DECEMBER 14, 2019

MANUSCRIPT HANDLED BY FABRIZIO NESTOLA

Endnote:

¹Deposit item AM-20-77136, Supplemental Material. Deposit items are free to all readers and found on the MSA website, via the specific issue’s Table of Contents (go to http://www.minsocam.org/MSA/AmMin/TOC/2020/Jul2020_data/Jul2020_data.html).